RSC Advances

ROYAL SOCIETY OF CHEMISTRY

www.rsc.org/advances

Multi-walled carbon nanotubes induced co-continuity of poly(ether ether ketone)/polyimide blends for high performance conductive materials

Cong Gao, Shuling Zhang, Bing Han, Hejing Sun, Guibin Wang, Zhenhua Jiang*

Alan G. MacDiarmid Institute, College of Chemistry, Jilin University,

Changchun 130012, People's Republic of China

*Correspondence author: Tel/Fax: (+86) 0431-85155361

E-mail: jiangzhenhua@jlu.edu.cn

Abstract:

A high performance conductive material with excellent mechanical and thermal properties was prepared by melt-blending, and its performance was adjusted by controlling the selective location of multi-walled carbon nanotubes (MWCNTs) in poly(ether ether ketone) (PEEK)/thermoplastic polyimide (TPI) matrix. With increasing the content of MWCNTs, the morphology of PEEK/TPI blends was changed from typical sea-island morphology to co-continuous structure, which was owing to the selective location of MWCNTs in TPI phase. Notably, the electrical percolation threshold was reduced to as low as 0.6 wt% due to the selective distribution of MWCNTs in the induced co-continuous PEEK/TPI structure, which is the lowest value reported for PEEK-based MWCNTs composites. Moreover, the introduction of MWCNTs could improve the dynamic mechanical property and thermal stability of PEEK/TPI blend effectively.

Key word: carbon nanotubes, immiscible polymer blends, electrical properties, double percolation

1. Introduction:

Nowadays, conductive materials have shown increasing attention in various areas, such as electrical conductive material, electro-chromic display, electromagnetic interference shielding and photovoltaic conversion.[1-4] Compared with traditional metal conductive materials, polymer-based conductive materials have attracted popularity in recent years because of their light weight, resistance to corrosion, flexibility, and processing advantages.[5-8] In the developed fields of polymer-based conductive materials, high performance polymers are of great interest. They are sought as an alternative for metals in the field of aerospace technology and energy industry because of their outstanding properties.[9-11]

Poly(ether ether ketone) (PEEK) and Nanjing Yuezi thermoplastic polyimide—YZPI^{TM} polyimide (TPI) are two typical high performance polymers with outstanding properties, such as superior mechanical properties and thermal stability.[12] Blending PEEK with TPI is an efficient strategy to combine the complementary properties of both polymers, it has been proven to improve the modulus at elevated temperature of the former and the chemical resistance and processability of the latter.[13] And PEEK/TPI blend is believed to be an ideal polymeric matrix for high performance conductive materials. However, as PEEK and TPI are immiscible with each other, the performance of PEEK/TPI blends is determined not only by properties of component polymers, but also by the morphology formed.[14-16] In recent years, much efforts have been devoted to polymer blends with a co-continuous structure due to their substantially improved properties, including electrical and thermal conductivity, elastic modulus, and heat resistance.[17-19] How to form and stabilize a co-continuous domains in PEEK/TPI blend during the melt processing is still a challenge.

The addition of nanoparticles into immiscible polymer blends is an effective method in extending the phase co-continuity and obtaining a co-continuous morphology.[20-22] Wu et al. clarified the mechanism

of nanoparticle induced co-continuity in acrylonitrile-butadiene-styrene (ABS)/polyamide 6 (PA6) blends. [20] While carbon nanotubes (CNTs), which have been considered as ideal fillers for polymer composites owing to their unique electronic and mechanical properties, are arousing more and more interest in various areas such as conductive composites and fibers.[23-27] Compared with single-walled carbon nanotubes (SWCNTs), multi-walled carbon nanotubes (MWCNTs) showed quite low commercial price for industrial usage.[28] Zou et al. reported that adding only a small amount of acid treated MWCNTs could change the morphology of poly(p-phenylene sulfide) (PPS)/polyamide 66 (PA66) blends from sea-island to co-continuous structure, which was mainly attributed to the selectively location of MWCNTs in the PA 66 phase.[22]

More importantly, though several methods for the preparation of PEEK/CNTs composites have been reported,[29-34] how to reduce the electrical percolation threshold of PEEK/MWCNTs composites remains challenging, while selective location of MWCNTs in immiscible polymer blends is a promising method to enhance the electrical properties at low MWCNTs loading.[17,35] Low MWCNTs loading means relatively low melt viscosity and improved impact resistance, as well as low cost to the final products. An electrical conductive material with very low filler content can be obtained by creating a co-continuous structure in the blend, which is called double percolation phenomenon.[36-38] Double percolation refers to the percolation of MWCNTs within one phase of the continuous polymer blend (first percolation), which itself percolates in the blend (second percolation). The reduction of percolation threshold in the double percolation system could be explained by the difference in the affinity of MWCNTs to the polymer components, which results in the MWCNTs selectively located in one of the two polymer phases. Meincke et al. reported that ABS/PA6/MWCNTs composites exhibited a highly irregular morphology in which MWCNTs were selectively distributed in the PA6 phase.[37] The

ABS/PA6/MWCNTs composites showed higher electrical conductivity at lower filler loading compared to PA6/MWCNTs or ABS/MWCNTs composites, which was attributed to the double percolation effect. MWCNTs-filled immiscible polymer composites with lower percolation threshold are cost-effective materials which can be manufactured on a large scale and widely used in positive temperature coefficient (PTC) materials, electromagnetic interference shielding and composite bipolar plates.[39-41] Based on the above analysis, PEEK/TPI and MWCNTs were respectively chosen as the polymer matrix and the filler to prepare a high performance conductive material with low percolation threshold and excellent comprehensive properties. Different ratios of MWCNTs were added into the PEEK/TPI matrix, and PEEK/TPI/MWCNTs composites were fabricated by melt extrusion. The selective distribution of MWCNTs in PEEK/TPI matrix and the morphological changes induced by adding MWCNTs were investigated. Moreover, the effects of MWCNTs on the electrical, mechanical and thermal properties of PEEK/TPI blend were discussed in detail.

2. Experimental

2.1. Materials

Poly(ether ether ketone) (PEEK) was supplied by Changchun Jilin University Super Engineering Plastics Research Co., Ltd. (P.R. China), the chemical structure of PEEK is shown in Figure 1a. YZPI^{TM} polyimide (TPI) was purchased from Nanjing Yuezi Chemical Col., Ltd. (P.R. China), and its chemical structure for reference is shown in Figure 1b. The inherent viscosity of PEEK was 0.63 dL.g^{-1} in H_2SO_4, and the inherent viscosity of TPI was 0.33 dL.g^{-1} in DMAc, determined with an Ubbelohde viscometer at 25 ^{o}C. MWCNTs grown by chemical vapor deposition were obtained from Chengdu Organic Chemicals Co., Ltd. (P.R. China). The outside diameter of the MWCNTs was ~15 nm, and the purity of the MWCNTs was greater than 95 wt%.

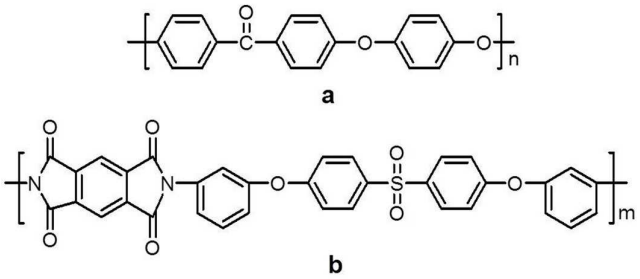

Figure 1. Structure of (a) PEEK and (b) TPI.

2.2. Sample preparation

PEEK/TPI/MWCNTs composites were prepared by melt blending. First, PEEK, TPI and MWCNTs were pre-mixed with a high-speed mixer for 2 min. Polymers and MWCNTs were dried in a vacuum oven at 120 ^{o}C for 24 h before use. Then, the pre-dispersion mixtures were blended using a Mini-Haake co-rotating twin-screw extruder at a screw speed of 80 rpm and a temperature of 355 ^{o}C. The detailed sample names and corresponding components for PEEK/TPI/MWCNTs composites are listed in Table 1. Moreover, binary PEEK/MWCNTs and TPI/MWCNTs composites with 2 wt% MWCNTs were also prepared by the same procedures for comparative experiments. Finally, the obtained samples were cut into granules, dried at 120 ^{o}C for 6 h, and then molded by Haake MiniJet for different measurements.

Table 1. Sample names and corresponding components for PEEK/TPI/MWCNTs composites

Samples names	PEEK/TPI/MWCNTs (wt%)
P/T	50/50
P/T/0.4%-CNTs	49.8/49.8/0.4
P/T/0.6%-CNTs	49.7/49.7/0.6
P/T/0.8%-CNTs	49.6/49.6/0.8
P/T/1%-CNTs	49.5/49.5/1
P/T/2%-CNTs	49/49/2
P/T/3%-CNTs	48.5/48.5/3

2.3. Characterization

The surface free energies of all the components were deduced by the contact angle measurements which were carried out on the surface of compression-molded films of PEEK and TPI. Contact angle

was measured at 20 ^{o}C on a JC2000C2 static contact angle measurement instrument. Double distilled water (H_2O) and methylene iodide (CH_2I_2) were used as probe liquids and measurement of a given contact angle was carried out at least 5 times.

Scanning electron microscopy (SEM) observation was performed using a HITACHI-SU8020 field emission scanning electron microscope operating at a 3.0 KV accelerating voltage. The selective extraction by DMAc for 24 h was firstly achieved to remove the TPI from some samples. The samples were dried and surfaces were then gold-sputtered before scanning.

Transmission electron microscopic (TEM) images were taken on a JEM-1200EX electron microscope operated at an acceleration voltage of 100 KV. The sample preparation involved embedding membranes in an Epon 812-Araldite mixture followed by ultramicrotomy with a diamond knife to obtain 80 nm thin sections which placed on copper grides for TEM analysis.

The alternating current (AC) conductivity were measured at room temperature in the frequency range between 10^2 and 10^6 Hz using an Aglient 4294A precision impedance analyzer. The samples were cut into small round specimens with a diameter of 10 mm, and two opposite surfaces of samples were coated with silver conductive glue to reduce the contact resistance between samples and electrodes.

Dynamic mechanical analysis (DMA) was carried out with a TA Instruments DMA Q800 in the tensile mode under N_2 atmosphere. All the measurements were performed in the linear with the strain of 0.03 %. Storage modulus of all samples were recorded at a frequency of 1 Hz and a heating rate of 5 $^{o}C \cdot min^{-1}$.

Thermal gravimetric analysis (TGA) was conducted under air atmosphere at a heating rate of 10 $^{o}C \cdot min^{-1}$. Samples of 3-5 mg were contained within open platinum pans of a PerkinElmer TGA-7 instrument.

3. Results and discussion

3.1. Selective location of MWCNTs

The selective distribution of MWCNTs in a specific phase or at the interface for an immiscible polymer blend is governed by thermodynamic factors. Wetting coefficient ω_a is proposed to define the selective distribution of MWCNTs according to the Young's equation[42]:

$$\omega_a = \frac{\gamma_{MWCNTs-polymer1} - \gamma_{MWCNTs-polymer2}}{\gamma_{polymer1,2}} \quad (1)$$

where $\gamma_{MWCNTs\text{-}polymer1}$, $\gamma_{MWCNTs\text{-}polymer2}$ and $\gamma_{polymer1,2}$ are the interfacial tensions between MWCNTs and polymer 1, between MWCNTs and polymer 2, and between the two polymers. If $\omega_a > 1$, MWCNTs preferentially distributed in polymer 2; if $-1 < \omega_a < 1$, MWCNTs distributed at the interface between the two phases, and if $\omega_a < -1$, MWCNTs preferentially distributed in polymer 1. The interfacial tensions γ_{12} can be calculated from the surface free energy according to the harmonic-mean equation and geometric-mean equation, respectively[43]:

$$\gamma_{12} = \gamma_1 + \gamma_2 - 4\left(\frac{\gamma_1^d \gamma_2^d}{\gamma_1^d + \gamma_2^d} + \frac{\gamma_1^p \gamma_2^p}{\gamma_1^p + \gamma_2^p}\right) \quad (2)$$

$$\gamma_{12} = \gamma_1 + \gamma_2 - 2\left(\sqrt{\gamma_1^d \gamma_2^d} + \sqrt{\gamma_1^p \gamma_2^p}\right) \quad (3)$$

where γ_1, γ_2 are the surface energies of polymer 1 and 2, γ_1^d and γ_2^d are the dispersive part and γ_1^p and γ_2^p are the polar part of the surface energies of polymer 1 and 2, respectively. The surface free energy can be calculated according to the harmonic-mean method[44]:

$$(1+\cos\theta_{H_2O})\gamma_{H_2O} = 4\left(\frac{\gamma_{H_2O}^d \gamma^d}{\gamma_{H_2O}^d + \gamma^d} + \frac{\gamma_{H_2O}^p \gamma^p}{\gamma_{H_2O}^p + \gamma^p}\right) \quad (4)$$

$$(1+\cos\theta_{CH_2I_2})\gamma_{CH_2I_2} = 4\left(\frac{\gamma_{CH_2I_2}^d \gamma^d}{\gamma_{CH_2I_2}^d + \gamma^d} + \frac{\gamma_{CH_2I_2}^p \gamma^p}{\gamma_{CH_2I_2}^p + \gamma^p}\right) \quad (5)$$

Where θ_{H2O} and θ_{CH2I2} is the contact angle to double distilled water (H_2O) and methylene iodide (CH_2I_2)

respectively, $\gamma = \gamma^d + \gamma^p$, $\gamma_{H2O} = \gamma_{H2O}^d + \gamma_{H2O}^p$, $\gamma_{CH2I2} = \gamma_{CH2I2}^d + \gamma_{CH2I2}^p$. The surface energy date are γ_{H2O}^d = 22.5 dyn cm^{-1} and γ_{H2O}^p = 50.8 dyn cm^{-1} for H_2O, and γ_{CH2I2}^d = 48.5 dyn cm^{-1} and γ_{CH2I2}^d = 2.3 dyn cm^{-1} for CH_2I_2.[45] Therefore, we can calculate surface free energies by measuring the contact angles of H_2O and CH_2I_2 on the surface of polymers.

In this work, the contact angle of H_2O and CH_2I_2 on the surfaces of PEEK and TPI were 87.36^o and 93.15^o for H_2O, and 40.45^o and 59.70^o for CH_2I_2. According to Eq. 4 and 5, the calculated surface free energies are shown in Table 2. For MWCNTs without modification, the corresponding surface energy data was suggested to be 27.8 mJ m^{-2} for γ, 17.6 mJ m^{-2} for γ^d and 10.2 mJ m^{-2} for γ^p.[46] The interfacial tensions between components were then calculated according to Eq. 2 and 3, and the results are shown in Table 3, the interfacial tension between PEEK and MWCNTs was calculated to be much higher than that between TPI and MWCNTs. Finally, the wetting coefficient ω_a for MWCNTs in PEEK/TPI blend could be calculated according to Eq. 1, it is clearly seen from Table 4 that both the harmonic- and geometric-mean predicted the MWCNTs would be in the TPI phase.

Table 2. Surface free energies γ of the samples [a]

Samples	γ (mJ m^{-2})	γ^d (mJ m^{-2})	γ^p (mJ m^{-2})
PEEK	42.1	36.2	5.9
TPI	32.8	27.3	5.5
MWCNTs	27.8	17.6	10.2

[a] $\gamma = \gamma^d + \gamma^p$. γ^d: dispersive component of γ. γ^p: polar component of γ.

Table 3. Interfacial tensions γ_{12} calculated using harmonic- and geometric-mean equation [b]

Materials pair	γ_{12}^h (mJ m^{-2})	γ_{12}^g (mJ m^{-2})
PEEK/MWCNTs	3.90	7.14
TPI/MWCNTs	1.78	3.51
PEEK/TPI	0.64	1.26

[b] The superscripts h and g represent the values calculated using harmonic- and geometric-mean equation, respectively.

Table 4. Wetting coefficient ω_a and predicted localization of MWCNTs in the PEEK/TPI blends [c]

System	ω_a^h	ω_a^g	predicted localization

PEEK/TPI/MWCNTs	3.31	2.88	TPI phase

[c] The superscripts w and o represent the values calculated using harmonic- and geometric-mean equation, respectively.

To further investigate the location of MWCNTs, comparative experiment was performed, as shown in Figure 2. Figure 2b is the magnified SEM image of the dotted-line circle of Figure 2a, which is the un-etched fractured surface of PEEK/TPI/MWCNTs composite. In some areas of Figure 2b, the skeleton of MWCNTs can be observed clearly and even some heads of MWCNTs were exposed. On the other hand, to distinguish the PEEK from TPI clearly, TPI on the fractured surface was etched by DMAc before the SEM test was taken. Figure 2d is the magnified SEM image of the dotted-line circle of Figure 2c, which is the etched fractured surface of PEEK/TPI/MWCNTs composite. The grey areas in Figure 2c are the PEEK phase and the black areas are the etched TPI phase. In contrast with Figure 2b, no MWCNTs could be observed in PEEK phase in Figure 2d. Therefore, it is clear that PEEK was the MWCNTs-free phase, and MWCNTs were selectively located in the TPI phase of PEEK/TPI matrix. The selective location of MWCNTs can also be evidenced by the TEM image of PEEK/TPI/MWCNTs with 1 wt% MWCNTs (Figure 3). Compared with traditional MWCNTs distribution in one-phase matrix,[36] MWCNTs in Figure 3a were selectively distributed in PEEK/TPI matrix and a co-continuous structure was formed. Moreover, the magnified dotted-line circle in Figure 3a demonstrated that the MWCNTs were well dispersed and the percolating network was formed (Figure 3b).

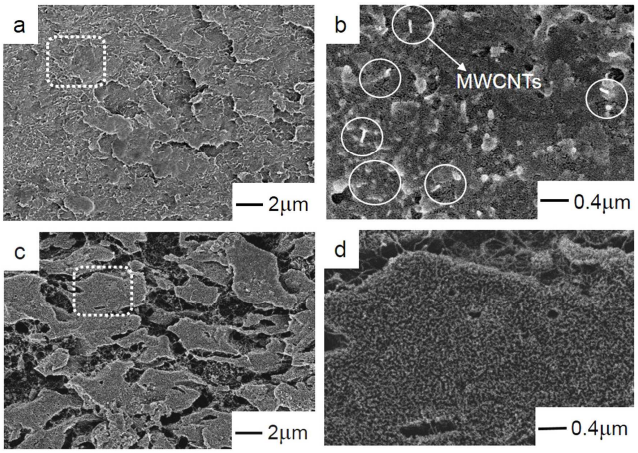

Figure 2. SEM images of (a) un-etched fractured surface of P/T/1%-CNTs, (b) magnified micrograph of the dotted-line circle region of (a), (c) etched fractured surface of P/T/1%-CNTs, (d) magnified micrograph of the dotted-line circle region of (c).

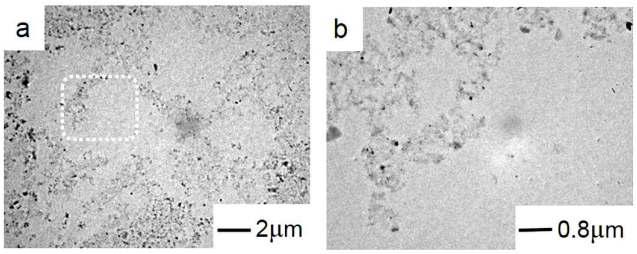

Figure 3. TEM images of (a) P/T/1%-CNTs, (b) magnified micrograph of the dotted-line circle region.

This heterogeneous distribution of MWCNTs in the two phases was due to the difference in the affinity of the MWCNTs to each component of the PEEK/TPI blends.[47,48] Owing to the sulphone group and the unsymmetrical structure of the TPI chain, TPI showed much better interfacial energies and wetting coefficient to MWCNTs than PEEK. Thermodynamically, MWCNTs tended to be located in the TPI phase with which it had lower interfacial tension. As noncovalent π-π interaction between aromatic polymers and unmodified MWCNTs was believed to be the main interaction, it is suggested that the π-π interaction between TPI and MWCNTs was much stronger that that between PEEK and MWCNTs.[49-51] Therefore, PEEK/TPI blend was proven to be an ideal matrix for the selective location of MWCNTs.

3.2. Morphological changes of PEEK/TPI blends

The selective location of MWCNTs resulted in great morphological changes of PEEK/TPI blends. Figure 4 shows the SEM micrograph of cryogenically fractured surface of PEEK/TPI blend and its MWCNTs-filled composites with different contents of MWCNTs. The PEEK/TPI blend without MWCNTs (Figure 4a) exhibited typical sea-island morphology, in which TPI domains were dispersed in the PEEK matrix. With the addition of MWCNTs, the phase morphology of PEEK/TPI was significantly changed. It can be seen that the morphology of PEEK/TPI was changing from sea-island to co-continuous like structure (Figure 4b and Figure 4c) when 0.4 wt% and 0.8 wt% MWCNTs was introduced in the PEEK/TPI matrix. With the further addition of 1 wt% MWCNTs, TPI phase formed a continuous phase and at the same time PEEK phase was still continuous (Figure 4d), which means a co-continuous structure was formed. With increasing the content of MWCNTs to 2% and 3%, the typical co-continuous morphology kept stable (Figure 4e and Figure 4f).

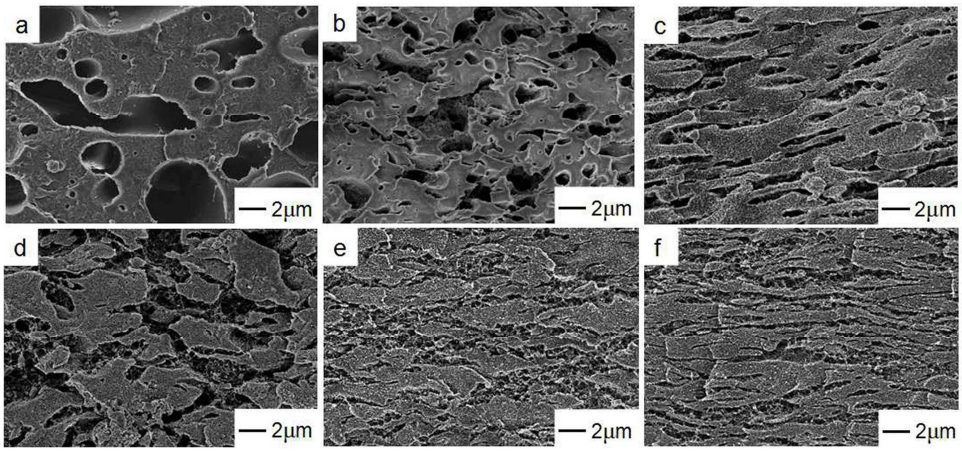

Figure 4. SEM images of PEEK/TPI composites with different contents of MWCNTs. (a) P/T, (b) P/T/0.4%-CNTs, (c) P/T/0.8%-CNTs, (d) P/T/1%-CNTs, (e) P/T/2%-CNTs, (f) P/T/3%-CNTs.

The mechanism of nanoparticle-induced phase inversion from a sea-island structure to a co-continuous one can be expressed as[52]

$$\frac{\phi_1}{\phi_2} = \frac{\eta_1}{\eta_2} \quad (6)$$

Whereφ_i and η_i is the volume fraction and melt viscosity of component i, respectively. That is an increase in the volume fraction or a decrease in viscosity of the minor polymer would enhance its continuity in the matrix. Firstly, the melt viscosity of TPI was higher than that of PEEK, thus forming a sea-island structure (Figure 4a). Then, the selective location of MWCNTs in TPI phase gave additional volume to the TPI phase, and according to Eq. 6, a co-continuous structure was formed with increased loading of MWCNTs (Figure 4d). Further increased MWCNTs loadings lead to a more stable co-continuous structure with delayed coarsening-driven break-up of the co-continuous structure (Figure 4f). This is because further increased MWCNTs loadings would evidently increase the viscosity of MWCNTs-localized TPI phase, thus the coarsening and phase coalescence of the TPI domains were suppressed and the phase co-continuity domains were stablized.[53] The process of phase morphology assembling in PEEK/TPI blend induced by adding MWCNTs can be summarized in Figure 5. MWCNTs were incorporated to act as a modifier to mediate the co-continuity of the PEEK/TPI blends effectively.

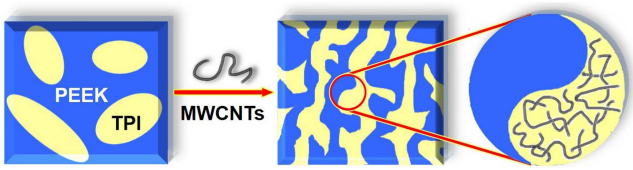

Figure 5. Schematic representation of MWCNTs induced co-continuity of PEEK/TPI blend.

3.3. Electrical properties

Polymer nanocomposites require a critical concentration of conductive nanofiller known as the electrical percolation threshold to transfer from the insulating state to the conductive state.[54] At the percolation concentration, the electrical conductivity of nanocomposites suddenly increases by several orders of magnitude. The increase in the conductivity at the percolation threshold depends on many

factors, in which the filler aspect ratio and the filler distribution are two key points.[55]

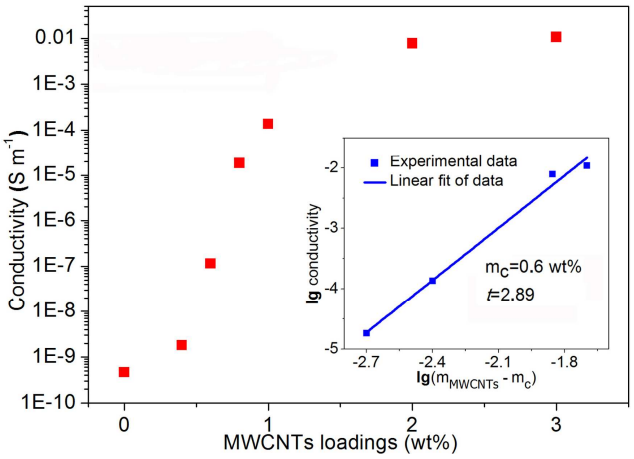

Figure 6. Dependence of the conductivity of PEEK/TPI/MWCNTs composites on the MWCNTs loadings at 10^3 Hz. The insert indicated the linear fit of conductivity to Eq. 7.

Figure 6 shows the electrical conductivity as a function of MWCNTs loadings for the ternary composites. For the PEEK/TPI blend, the bulk conductivity was rather low, less than 10^{-9} S m^{-1}, and the 0.4 wt% addition of MWCNTs had little effect on the electrical conductivity, which means that 0.4 wt% MWCNTs was not enough to provide the conductive network in the composites. However, an obvious increase in conductivity by nearly 4 orders of magnitude was observed between 0.4 wt% and 0.8 wt% MWCNTs were added, where the conductivity changed rapidly from 1.8×10^{-9} S m^{-1} to 1.84×10^{-5} S m^{-1}. This significant increase in electrical conductivity was attributed to the double percolation phenomenon. With the content of MWCNTs increased from 0.4 wt% to 0.8 wt%, the morphology changed from sea-island to co-continuous structure, which ensured the continuity of MWCNTs selected located TPI phase, as evidenced by Figure 2. It is suggested that MWCNTs in TPI phase was forming the conductive network, and TPI phase itself was forming the conductive network in the whole composites. Further increasing the MWCNTs concentration to above 0.8% yielded a relatively gradual rise in electrical conductivity, with 1.35×10^{-4} S m^{-1} at 1 wt% and 7.73×10^{-3} S m^{-1} at 2

wt%. Compared with other polymers/MWCNTs composites, the PEEK/TPI/MWCNTs composites showed relatively low electrical conductivity, this should be owing to the high melt viscosity and melt temperature of the super-engineering plastics (PEEK and TPI), which affected the good dispersion of MWCNTs in the polymer matrix.[9, 12, 30] The change in electrical conductivity of PEEK/TPI/MWCNTs composites, σ, can be fitted above the percolation using the Power law[56]:

$$\sigma \propto \sigma_0 \left(\mathrm{m}-\mathrm{m}_c\right)^t \quad (7)$$

Where σ_0 is the bulk electrical conductivity of the filler, m is the filler mass fraction, m_c is the electrical percolation threshold, and t is the universal critical exponent describing the rapid variation of σ near percolation threshold (m_c). The best fit to the data was obtained for a percolation threshold $m_c = 0.006$ and $t = 2.89$, as shown in Figure 6. Moreover, it is worth noting that the percolation threshold obtained (0.6 wt%) is the lowest value compared with that reported for PEEK-based MWCNTs nanocomposites fabricated by melt blending (1.3 wt% and 3.5 wt%).[29,30] This low percolation threshold could be attributed to the selective location of MWCNTs and the formation of the co-continuous structure.

The dependency of the AC conductivity of PEEK/TPI/MWCNTs composites on the frequency is presented in Figure 7(a). Apparently, the AC conductivity of PEEK/TPI/MWCNTs composites increased almost linearly with increasing the frequency when the content of MWCNTs was lower than 0.6 wt%, which demonstrated their insulating behavior.[57] In contrast, when the content of MWCNTs reached 0.8 wt%, the conductivity of the composite exhibited a typical curves of semiconductors, which appeared a plateau at first and then increased a little at high-frequency regime. With further increasing the content of MWCNTs to above 1 wt%, the conductivity of the composites became independent on frequency which ranged from 100 Hz to 1 MHz. This could be attributed to the content of MWCNTs was enough to effectively provide the tunnel for the hop of electrons.

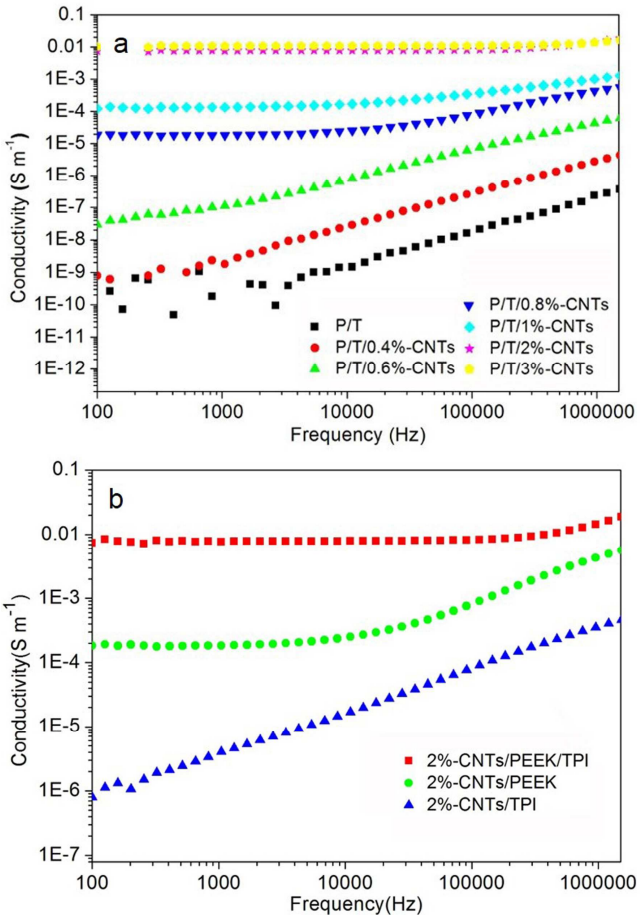

Figure 7. (a) Dependence of AC conductivity of PEEK/TPI/MWCNTs composites with different MWCNTs content on frequency. (b) Dependence of AC conductivity of different polymer-based composites with 2 wt% MWCNTs on frequency.

To further confirm the superior conductivity of PEEK/TPI/MWCNTs composites, the AC conductivity of different polymer-based composites with the same MWCNTs loading (2 wt%) was shown in Figure 7(b). Mention that the conductivity of PEEK/TPI/MWCNTs (m_c = 0.6 wt%) was expected to be obviously better than that of binary composites below the percolation of PEEK/MWCNTs (1.3 wt%), so a relatively higher MWCNTs loading (2 wt%) was chosen to compare the conductivity, which would be more persuasive. As shown in Figure 7(b), the AC conductivity of TPI/MWCNTs composites with 2 wt% MWCNTs increased almost linearly with increasing the frequency, which was a typical insulating

behavior. While the PEEK/MWCNTs composite showed a typical semiconductors behavior, the conductivity of which appeared a plate at first and then increased at high frequency regime. The difference of conductivity between PEEK and TPI composites was owing to the discrepant melt viscosity and processing fluidity. PEEK showed better melt fluidity than TPI, so it was relatively easier to obtain a good dispersion of MWCNTs in PEEK matrix. With the same content of MWCNTs, the ternary PEEK/TPI/MWCNTs composites possessed the best conductive property compared with binary PEEK/MWCNTs and TPI/MWCNTs composites. The PEEK/TPI/MWCNTs composite with 2 wt% MWCNTs almost became a conductive material, of which the conductivity was independent of the frequency. Moreover, the conductivity of the ternary composites (PEEK/TPI/MWCNTs) at 10^3 Hz was far higher than that of the binary ones (PEEK/MWCNTs and TPI/MWCNTs) by about 50 and 2000 times respectively. This suggested the good electrical property should be attributed to the double percolation phenomenon.

3.4. Dynamic mechanical property and thermal stability

Dynamic mechanical analysis (DMA) was introduced to investigate the changes of the tensile modulus with temperature. Storage modulus measured by DMA is regarded as the maximum energy stored in the material during one cycle of oscillation, and represents the stiffness and elastic nature of the material.[58] The variation of storage modulus curves as a function of temperature for PEEK/TPI and its MWCNTs composites are presented in Figure 8. It can be seen that the storage modulus values of the PEEK/TPI/MWCNTs composites were obviously higher than that of neat PEEK/TPI blend at the same temperature. With increasing MWCNTs loading level, the storage modulus of the PEEK/TPI/MWCNTs composites increased gradually. In the range of 40-150 ^{o}C, the storage modulus of PEEK/TPI blend was about 1830 MPa, while the storage modulus of PEEK/TPI/MWCNTs with merely 0.4 wt% of

MWCNTs reached around 2080 MPa, and it continued to increase to 2180 MPa and 2340 MPa with 1 wt % and 3 wt% MWCNTs, respectively. In the range of 150-200 ^{o}C, there was a sharp decrease of storage modulus, which was mainly due to decrease of the storage modulus of PEEK at above its T_g (143 ^{o}C). Moreover, the storage modulus of PEEK/TPI/MWCNTs composites with different content of MWCNTs was obviously higher than that of PEEK/TPI blend. In the case of the storage modulus at 185 ^{o}C, the storage modulus of PEEK/TPI blend was 907 MPa, whereas the storage modulus of PEEK/TPI/MWCNTs with 1 and 3 wt% MWCNTs attained 1127 MPa and 1180 MPa, respectively. In the range of 200-240 ^{o}C, the storage modulus of PEEK/TPI blend was 594 MPa, whereas the storage modulus of PEEK/TPI/MWCNTs with 0.4 and 3 wt% MWCNTs reached 780 MPa and 855 MPa, which exhibits 31 % and 44 % increase, respectively. The significant improvement in storage modulus of PEEK/TPI/MWCNTs was mainly ascribed to the stiffening effect of the carbon nanotubes,[59,60] which was particularly significant at elevated temperature. In short, MWCNTs was an effective filler to improve the storage modulus of PEEK/TPI blend, especially at elevated temperature. Only 0.4 wt% MWCNTs could increase the storage modulus of PEEK/TPI blend by 31 % in the range of 200-240 ^{o}C.

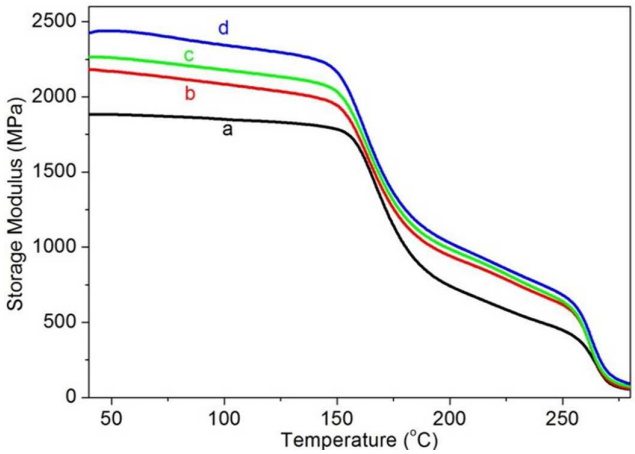

Figure 8. Storage modulus curves of (a) P/T, (b) P/T/0.4%-CNTs, (c) P/T/1%-CNTs and (d) P/T/3%-CNTs.

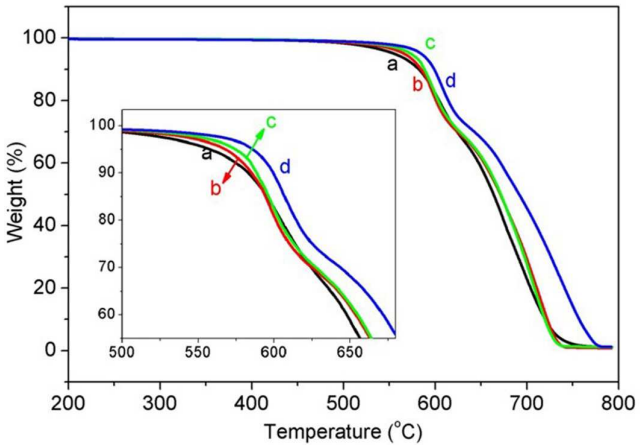

Figure 9. TGA curves of (a) P/T, (b) P/T/0.4%-CNTs, (c) P/T/1%-CNTs and (d) P/T/3%-CNTs.

To investigate the effect of adding MWCNTs on thermal stability of PEEK/TPI blend and its CNTs composites, TGA was performed under air atmosphere. The thermo-degradation curves of PEEK/TPI blend and PEEK/TPI composites containing different contents of MWCNTs are shown in Figure 9. It can be seen that the thermal stability of PEEK/TPI composites with MWCNTs were much superior compared with that of PEEK/TPI blend. The 5% and 10% weight loss temperature ($T_d^{5\%}$ and $T_d^{10\%}$) of PEEK/TPI blend were 558 ^oC and 583 ^oC, whereas the $T_d^{5\%}$ and $T_d^{10\%}$ of P/T composites with 0.4 wt% CNTs reached 568 ^oC and 585 ^oC, respectively. This may attributed to MWCNTs restricting of thermal mobility of polymer chains, thereby making the composites more thermally stable.[9, 61] Simultaneously, the selective location of MWCNTs and the formation of MWCNTs network structure might also benefit the thermal stability of the PEEK/TPI/MWCNTs. Moreover, the P/T/3%-CNTs composites presented excellent thermal stability, the $T_d^{5\%}$ and $T_d^{10\%}$ of P/T/3%-CNTs were 586 ^oC and 600 ^oC respectively, which was 18 ^oC and 17 ^oC higher than that of P/T blend without MWCNTs. These results indicated that the incorporation of MWCNTs could improve the thermal stability of PEEK/TPI blend effectively, the $T_d^{5\%}$ under air atmosphere of PEEK/TPI/MWCNTs composites was all above 568 ^oC, which indicated the outstanding thermal stability of this material.

4. Conclusion

A novel conductive material with excellent comprehensive properties based on PEEK/TPI/MWCNTs composites was fabricated by direct melt blending. MWCNTs were selectively located in TPI phase due to different affinity of the MWCNTs to PEEK and TPI. The selectively located MWCNTs induced great morphological changes of PEEK/TPI blend from typical sea-island morphology to co-continuous structure. Notably, the electrical percolation threshold was reduced to as low as 0.6 wt% due to the selective distribution of MWCNTs in the induced co-continuous PEEK/TPI structure, which is the lowest value reported for PEEK-based MWCNTs composites fabricated by melt extrusion. Moreover, merely 0.4 wt% content of MWCNTs could increase the storage modulus by 31% in the range of 200-240 ^{o}C, and the 5% weigh loss temperature under air atmosphere of PEEK/TPI/MWCNTs composites was all above 568 ^{o}C. In summary, a high performance conductive material with excellent electrical conductivity and good mechanical and thermal properties was obtained by controlling the MWCNTs induced co-continuity of PEEK/TPI blends. This structurally and functionally integrated material has promising applications in electromagnetic interference shielding and antistatic fields for aeronautics industry.

Acknowledgment

This work was financially supported by the National Natural Science Foundation of China (No. 51203060).

Reference

1 Y. Yang, M. C. Gupta, K. L. Dudley and R. W. Lawrence, *Nano Lett.*, 2005, **5**, 2123.

2 F. Zhang, M. Johansson, M. R. Andersson, J. C. Hummelen and O. Inganas, *Adv. Mater.*, 2002, **14**, 662.

3 M. Gratzel, *Nature*, 2001, **414**, 338.

4 A. Cihaner and F. Algi, Adv. *Funct. Mater.*, 2008, **18**, 3583.

5 M. F. Yu, O. Lourie, M. J. Dyer, K. Moloni, T. F. Kelly and R. S. Ruoff, *Science*, 2000, **287**, 637.

6 Y. J. Kim, T. S. Shin, H. D. Choi, J. H. Kwon, Y. C. Chung and H. G. Yoon, *Carbon*, 2005, **43**, 23.

7 A. Moisala, Q. Li, I. A. Kinloch and A. H. Windle, *Compos. Sci. Technol.*, 2006, **66**, 1285.

8 M. Moniruzzaman and K. I. Winey, *Macromolecules*, 2006, **39**, 5194.

9 H. Wang, G. Wang, W. Li, Q. Wang, W. Wei, Z. Jiang and S. Zhang, *J. Mater. Chem.*, 2012, **22**, 21232.

10 Y. C. Tseng and E. M. Woo, *Macromol. Rapid Commun.*, 1998, **19**, 215.

11 Z. Ounaies, C. Park, K. E. Wise, E. J. Siochi and J. S. Harrison, *Compos. Sci. Technol.*, 2003, 63, 1637.

12 C. Gao, S. Zhang, X. Li, S. Zhu and Z. Jiang, *Polymer*, 2014, **55**, 119.

13 http://kbam.geampod.com/KBAM/Reflection/Assets/15778.pdf

14 X. Kong, F. Teng, H. Tang, L Dong and Z. Feng, *Polymer*, 1996, **37**, 1751.

15 B. B. Sauer, B. S. Hsiao and K. L. Faron, *Polymer*, 1996, **37**, 445.

16 S. Swier, M. T. Shaw and R. A. Weiss, *J. Membrane Sci.*, 2006, **270**, 22.

17 C. Su, L. Xu, C. Zhang and J. Zhu, *Compos. Sci. Technol.*, 2011, **71**, 1016.

18 S. Wen and D. D. L. Chung, *Carbon*, 2007, **45**, 263.

19 R. Jung, W. I. Park, S. M. Kwon, H. S. Kim and H. J. Jin, *Polymer*, 2008, **49**, 2071.

20 G. Wu, B. Li and J. Jiang, *Polymer*, 2010, **51**, 2077.

21 D. Wu, Y. Zhang, M. Zhang and W. Yu, *Biomacromolecules*, 2009, **10**, 417.

22 H. Zou, K. Wang, Q. Zhang and Q. Fu, *Polymer*, 2006, **47**, 7821.

23 E. Frackowiak, K. Metenier, V. Bertagna and F. Beguin, *Appl. Phys. Lett*, 2000, **77**, 2421.

24 T. Liu, I. Y. Phang, L. Shen, S. Y. Chow and W. D. Zhang, *Macromolecules*, 2004, **37**, 7214.

25 A. Penicaud, L. Valat, A. Derre, P. Poulin, C. Zakri, O. Roubeau, M. Maugey, P. Miaudet, E. Anglaret, P. Petit, A. Loiseau and S. Enouz, *Compos. Sci. Technol.*, 2007, **67**, 795.

26 C. Jiang, A. Saha, C. Xiang, C. C. Young, J. M. Tour, M. Pasquali and A. A. Marti, *ACS Nano*, 2013, **7**, 4503.

27 C. Xiang, W. Lu, Y Zhu, Z. Sun, Z. Yan, C. Hwang and J. M. Tour, *ACS Appl. Mater. Inter.*, 2012, **4**, 131.

28 Q. Zhang, J. Q. Huang, W. Z. Qian, Y. Y. Zhang and F. Wei, *Small*, 2013, **9**, 1237.

29 D. S. Bangarusampath, H. Ruckdaschel, V. Altstadt, J. K. W. Sandler, D. Garray and M. S. P. Shaffer, *Chem. Phys. Lett.*, 2009, **482**, 105.

30 M. Mohiuddin and S. V. Hoa, *Compos. Sci. Technol.*, 2011, **72**, 21.

31 A. M. Diez-Pascual, M. Naffakh, C. Marco, G. Ellis and M. A. Gomez-Fatou, *Prog. Mater. Sci.*, 2012, **57**, 1106.

32 D. S. Bangarusampath, H. Ruckdaschel, V. Altstadt, J. K. W. Sandler, D. Garray and M. S. P. Shaffer, *Polymer*, 2009, **50**, 5803.

33 A. M. Diez-Pascual, M. Naffaka, M. A. Gomez, C. Macro, G. Ellis, J. M. Gonzalez-Dominguez, A. Anson, M. T. Martinez, Y. Martinez-Rubi, B. Simard and B. Ashrafi, *Nanotechnology*, 2009, **20**, 315707.

34 A. M. Diez-Pascual, M. Naffakh, J. M. Gonzalez-Domingues, A. Anson, Y. Martinez-Rubi, M. T.

Martinez, B. Simard and M. A. Gomez, *Carbon*, 2010, **48**, 3500.

35 M. Wu and L. L. Shaw, *J. Power Sources*, 2004, **136**, 37.

36 P. Potschke, A. R. Bhattacharyya and A. Janke, *Carbon*, 2004, **42**, 965.

37 O. Meincke, D. Kaempfer, H. Weickmann, C. Friedrich, M. Vathauer and H. Warth, *Polymer*, 2004, **45**, 739.

38 M. Q. Zhang, G. Yu, H. M. Zeng, H. B. Zhang and Y. H. Hou, *Macromolecules*, 1998, **31**, 6724.

39 J. W. Zha, W. K. Li, R. J. Liao, J. Bai and Z. M. Dang, *J. Mater. Chem. A*, 2013, **1**, 843.

40 J. Yun, J. S. Im, Y. S. Lee and H. I. Kim, *Eur. Polym. J.*, 2010, **46**, 900.

41 R. A. Antunes, M. C. L. de Oliveira, G. Ett and V. Ett, *J. Power Sources*, 2011, **196**, 2945.

42 M. Sumita, K. Sakata, S. Asai, K. Miyasaka and H. Nakagawa, *Polym. Bull.*, 1991, **25**, 265.

43 S. Wu, Polymer Interface and Adhesion, Marcel Dekker, New York, 1982.

44 D. K. Owens and R. C. Wendt, *J. Appl. Polym. Sci.*, 1969, **13**, 1741.

45 E. N. Dalai, *Langmuir*, 1987, **3**, 1009.

46 A. H. Barber, S. R. Cohen and H. D. Wagner, *Phys. Rev. Lett.*, 2004, **92**, 18610.

47 Z. Xu, Y. Zhang, Z. Wang, N. Sun and H. Li, *ACS Appl. Mater. Inter.*, 2011, **3**, 4858.

48 L. Zhang, C. Wan and Y. Zhang, *Compos. Sci. Technol.*, 2009, **69**, 2212.

49 B. Zhang, A. N. Chakoli, W. Zang, Y. Tian, K. Zhang, C. Chen and Y. Li, *J. Appl. Polym. Sci.*, 2014, DOI: 10.1002/APP.40479.

50 T. Kar, H. F. Bettinger, S. Scheiner and A. K. Roy, *J. Phys. Chem. C*, 2008, **112**, 20070.

51 Y. Jin, H. Liu, N. Wang, L. Hou and X. Zhang, *Mater. Chem. Phys.* 2012, **135**, 948.

52 D. R. Paul and J. W. Barlow, *J. Macromol. Sci. R. M. C.*, 1980, **18**, 109.

53 F. Gubbels, S. Blacher, E. Vanlathem, R. Jerome, R. Deltour, F. Brouers and P. Teyssie,

Macromolecules, 1995, **28**, 1559.

54 I. Balberg and N. Binenbaum, *Phys. Rev. Lett.*, 1984, **52**, 1465.

55 J. Li, P. C. Ma, W. S. Chow, C. K. To, B. Z. Tang and J. K. Kim, *Adv. Funct. Mater.*, 2007, **17**, 3207.

56 H. Leuenberger, *Adv. Powder Technol.*, 1999, **10**, 323.

57 M. T. Connor, S. Roy, T. A. Ezquerra and F. J. B. Calleja, *Phys. Rev. B*, 1998, **57**, 2286.

58 W. Wei, X. Yue, Y. Zhou, Z. Chen, J. Fang, C. Gao and Z. Jiang, *Phys. Chem. Chem. Phys.*, 2013, **15**, 21043.

59 M. S. P. Shaffer and A. H. Windle, *Adv. Mater.*, 1999, **11**, 937.

60 Z. Jin, K. P. Pramoda, G. Xu and S. H. Goh, *Chem. Phys. Lett.*, 2001, **337**, 43.

61 S. W. Ko, M. K. Hong, B. J. Park, R. K. Gupta, H. J. Choi and S. N. Bhattacharya, *Polym. Bull.*, 2009, **63**, 125.

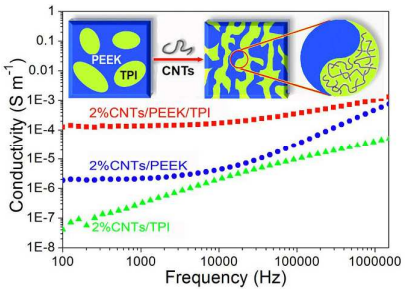

High performance conductive material was prepared based on MWCNTs induced co-continuity of PEEK/TPI blends.